https://doi.org/10.5194/bg-2023-140
Preprint. Discussion started: 22 September 2023

Biogeosciences Discussions

Elevated atmospheric CO_2 and vegetation structural changes contributed to GPP increase more than climate and forest cover changes in subtropical forests of China

Tao Chen[1, 2, *], Félicien Meunier[2], Marc Peaucelle[3], Guoping Tang[1, *], Ye Yuan[4], Hans Verbeeck[2]

1. Carbon-Water Research Station in Karst Regions of Northern Guangdong, School of Geography and Planning, Sun Yat-Sen University, Guangzhou 510006, China
2. CAVElab – Computational and Applied Vegetation Ecology, Department of Environment, Ghent University, Ghent 9000, Belgium
3. INRAE, Université de Bordeaux, UMR 1391 ISPA, 33140 Villenave-d'Ornon, France
4. State Key Laboratory of Desert and Oasis Ecology, Xinjiang Institute of Ecology and Geography, Chinese Academy of Sciences, Urumqi 830011, China

**Corresponding to:* Tao Chen (chent265@mail2.sysu.edu.cn); Guoping Tang (tanggp3@mail.sysu.edu.cn)

Abstract: The **s**ubtropical forest gross primary productivity (GPP) plays a pivotal role in the global carbon cycle and in regulating the global climate. Quantifying the individual and combined effects of forest cover change (FCC), vegetation structural change (VSC, i.e., leaf area index (LAI)), CO_2 fertilization, and climate change (CC) on annual GPP dynamics of various subtropical forest types are essential for mitigating carbon emissions and predicting climate changes, but these impacts remain unclear. In this study, we used a processed-based model to comprehensively investigate the impacts of these factors on GPP variations with a series of model experiments in China's subtropical forests during 2001-2018. Simulated actual GPP showed a significant increasing trend (26.72 TgC year^{-1}, $p < 0.001$) under the interaction effects of these factors. The CO_2 fertilization (8.23 TgC year^{-1}, $p < 0.001$) and VSC (4.55 TgC year^{-1}, $p = 0.005$) were the two dominant drivers of total subtropical forest GPP increase, followed by the effect of FCC (1.35 TgC year^{-1}, $p < 0.001$) and CC (1.11 TgC year^{-1}, $p = 0.08$). We observed different responses to drivers depending on forest types. The evergreen broadleaved forests have a high carbon sink potential due to the positive effects of all drivers. Both the FCC (1.29 TgC year^{-1}, $p < 0.001$) and CC (0.53 TgC year^{-1}, $p < 0.05$) significantly decreased evergreen needleleaved forest GPP, while their negative effects were almost offset by the positive impact of VSC. Our results indicated that forest structural change outweighed the forest cover change in promoting GPP, which is an overlooked driver that needs to be accounted for in studies, as well as ecological and management programs. Overall, our study offers a novel perspective on different drivers of subtropical forest GPP changes, which provides valuable information for policy makers in forest management to mitigate climate change.

Keywords: Subtropical forests, Gross primary production (GPP), Vegetation structure change, Climate change, BEPS process-based model

https://doi.org/10.5194/bg-2023-140
Preprint. Discussion started: 22 September 2023

Biogeosciences Discussions
Open Access
EGU

1. Introduction

Mitigating emissions through ecosystem carbon absorption is a potential solution to slow the increase of global atmospheric carbon dioxide (CO_2) concentration and temperature (Fang et al., 2014). Forest ecosystems, which cover about 30% of the global land area (Thornton et al., 2002), are one of the main terrestrial carbon sinks (Mathias and Trugman, 2022; Pan et al., 2011) through photosynthesis (Beer et al., 2010). China's forest ecosystems, with an area of approximately 1.95×10^6 km^2 (Li et al., 2014), are mainly distributed in the subtropical regions, which are an important component of the global forest ecosystems and crucial to the global and regional climate system (Fang et al., 2010; Yu et al., 2014). However, China is still one of the world's top emitters of greenhouse gases that directly contribute to global warming (Friedlingstein et al., 2022; Yu et al., 2014). Therefore, precise quantification of China's subtropical forest GPP and understanding of its driving mechanisms are of great importance for scientists and policy makers to mitigate climate change and carbon emissions with the carbon sink potential of the Chinese subtropical forests (Fang et al., 2010; Yu et al., 2014).

Several national key ecological restoration programs have been implemented in China to reverse land and environmental degradation (Lu et al., 2018), such as the natural and planted forest area increased by 2.3×10^7 ha and 2.6×10^7 ha during the past two decades, respectively (Chen et al., 2021b). Remote sensing observations have also identified the hotspots of forest gains and greening in southern China resulting from these programs' implements (Chen et al., 2019a; Tong et al., 2018). However, the subtropical regions are the most developed in China and have a very high population density with more than 10% (approximately 8.2 billion) of the world population. Intense land cover/use changes have become prominent in this region due to rapid industrialization and urbanization, leading to serious changes to forest ecosystems (e.g., LAI and GPP) (Chen et al., 2019b; Tong et al., 2018; Zhang et al., 2014). In addition, the annual mean temperature in the Chinese subtropical monsoon region has increased by more than 1.0 °C over the past 30 years, which was higher than the global average (Fang et al., 2018) and has also influenced the forest carbon uptake (Gao et al., 2017; Yuan et al., 2016). Meanwhile, the annual mean atmospheric CO_2 concentration in China has reached new highs due to large anthropogenic emissions (e.g., 407 ppm in 2017) (CMA, 2018), which also affected the photosynthetic rates, and thereby influenced the vegetation productivity (Chen et al., 2022a).

Recently, several studies investigated the roles of climate factors in regulating the changes of forest GPP at the site or global scales (Barman et al., 2014; Ma et al., 2015), as well as in some regions of China (Ma et al., 2019; Yao et al., 2018b). Some studies indicated that temperature was the major factor in forest GPP variations, while other studies suggested that precipitation and solar radiation were the key driving forces (Chen et al., 2021a; Fyllas et al., 2017; Li et al., 2022; Mo et al., 2018). Moreover, previous studies have also reported that LAI, as an important parameter of VSC can reflect the vegetation growth and land-use management (Chen et al., 2019a; Chen et al., 2019b), and CO_2 fertilization were the pivotal drivers for enhancing carbon sink in terrestrial vegetation, particularly of China's forest ecosystems (Chen et al., 2019b; Chen et al., 2021a). However, these studies in identifying the drivers of changes in forest GPP led to divergent conclusions. Moreover, most of the current studies mainly considered different forests as a single forest type, and attempted to untangle the individual and combined

https://doi.org/10.5194/bg-2023-140
Preprint. Discussion started: 22 September 2023

Biogeosciences
Discussions

impact of different factors on forest GPP changes (Chen et al., 2021a; Zhang et al., 2022). However, the relative contributions of these factors to China's subtropical forest GPP variations for specific forest types were still not clear.

In the past decades, different methods have been used to estimate vegetation GPP. The process-based models, especially in combination with remote sensing data (Chen et al., 2019b; Liu et al., 1997), are by far one of the most important tools for different forests by explicitly representing processes and their interaction with the environment and for disentangling the drivers of GPP variations over multiple spatiotemporal scales. The Boreal Ecosystem Productivity Simulator (BEPS) was developed based on the FOREST-BGC model (Running and Coughlan, 1988), which is a process-based diagnostic model and has the advantages of incorporating the remote sensing data (e.g., LAI and land cover type) to represent the solid biophysical processes. Recently, the BEPS model has been widely used at the regional and global scale and proved to be one of the better-performing models for forest GPP simulations (Chen et al., 2019b; Chen et al., 2012; Liu et al., 1997; Luo et al., 2019; Wang et al., 2021a), especially it has been well evaluated and validated in China (Feng et al., 2007; Liu et al., 2018; Peng et al., 2021; Wang et al., 2018) but has not been used to unravel the drivers of different forests changes.

Therefore, in this study, we especially focus on the subtropical forest ecosystems of China. The BEPS model was used to simulate different forest GPP. The specific objective of this study is to (1) test the performance of the BEPS model in simulating the GPP of the subtropical forest ecosystems, (2) quantify spatiotemporal trends in different GPP across the subtropical forests, and (3) disentangle the relative effects of the forest cover change, climate change, vegetation structure change, and CO_2 fertilization on different forest GPP variations in the study area. The results of this study may provide valuable information for scientists and policy makers.

2. Materials and methods

2.1 Study area description

In this study, we focused on China's subtropical forests which account for approximately 64% (~1.25 $\times 10^6$ km^2) of the total forested area in China, and the boundary of the subtropical region was derived from the Resource and Environment Science and Data Center of China (He et al., 2021a; He et al., 2019), which covers a latitudinal range of 21.33–33.91°N and a longitudinal range of 91.39–122.49°E and has a typical subtropical monsoon climate. The average annual temperature is about 15.5°C and the mean annual precipitation ranges from 800 mm in the north to more than 2000 mm in the south, with 80% of precipitation concentrated in the growing season. The main forest types in the subtropical region of China include the evergreen broadleaved forest (EBF), evergreen needle-leaved forest (ENF), deciduous broadleaved forest (DBF), and mixed forest (MXF) (Fig.1). There are three operating flux towers in the area: Qianyanzhou (QYZ), Dinghushan (DHS), and Ailaoshan (ALS). A more detailed description of these flux tower sites can be found in Table S1.

https://doi.org/10.5194/bg-2023-140
Preprint. Discussion started: 22 September 2023

Biogeosciences
Discussions

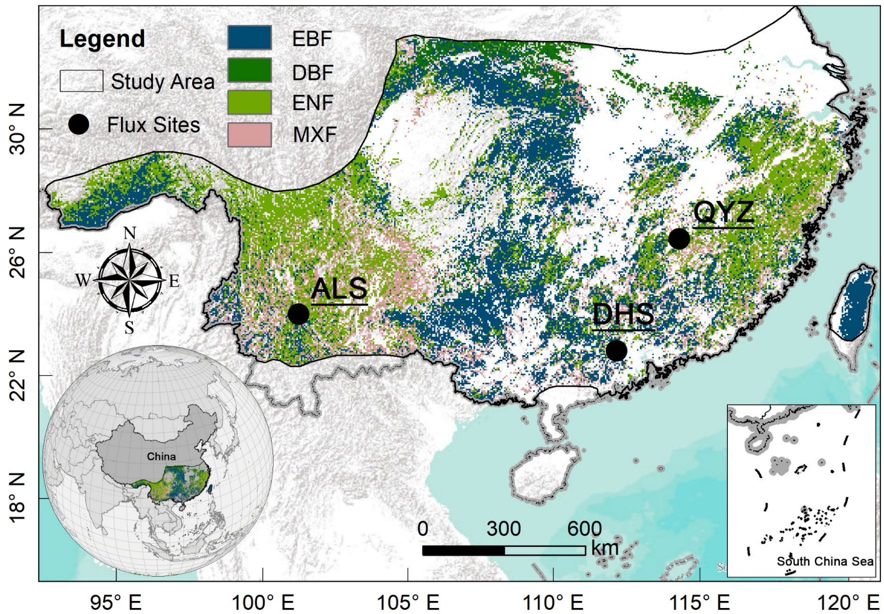

Figure 1 Location of the study area and 3 flux sites. The forest cover map (2018) shown here was derived from the European Space Agency land cover data (ESA CCI-LC). The forest types of ALS and DHS are EBF, and the forest type of QYZ is ENF.

2.2 Model description

In this study, we used the BEPS model to simulate the forest GPP and NEP with a resolution of 0.05°. The BEPS is a process-based model driven by the remotely sensed leaf area index (LAI), land cover types, soil data, and meteorological data. Recently, the BEPS model was used to simulate the terrestrial ecosystem carbon and water fluxes over different regions, such as the globe (Chen et al., 2019b; Chen et al., 2012), North America (Sprintsin et al., 2012; Xie et al., 2018), Europe (Wang et al., 2003), East Asia (Matsushita and Tamura, 2002), as well as the whole or southern China (Liu et al., 2018; Liu et al., 2014; Peng et al., 2021). A more detailed description of the original BEPS can be found in Supplementary section Text S1 and previous studies (Chen et al., 2019b; Chen et al., 1999; Ju et al., 2006; Liu et al., 1999; Liu et al., 1997). In BEPS, the daily GPP ($\mathrm{gC\ m^{-2} day^{-1}}$) is calculated as (Chen et al., 1999):

$$\mathrm{GPP = GPP_{sun}LAI_{sun} + GPP_{shade}LAI_{shade}} \tag{1}$$

where $\mathrm{GPP_{sun}}$ ($\mathrm{gC\ m^{-2} day^{-1}}$) and $\mathrm{GPP_{shade}}$ ($\mathrm{gC\ m^{-2} day^{-1}}$) denote the GPP per unit area of sunlit and shaded leaves; $\mathrm{LAI_{sun}}$ ($m^2\ m^{-2}$) and $\mathrm{LAI_{shade}}$ ($m^2\ m^{-2}$) respectively represent the LAI of sunlit and shaded leaves. $\mathrm{LAI_{sun}}$ and $\mathrm{LAI_{shade}}$ depend on the mean solar zenith angle (θ, unitless):

$$\mathrm{LAI_{sun}} = 2\cos\theta \times (1 - \exp(-0.5\Omega \mathrm{LAI}/\cos\theta)) \tag{2}$$

$$\mathrm{LAI_{shade}} = \mathrm{LAI} - \mathrm{LAI_{sun}} \tag{3}$$

where LAI is the total canopy leaf area index ($m^2\ m^{-2}$) and Ω is the clumping index (unitless).

In the BEPS model, the maximum carboxylation rate V_{cmax} (μmol $m^{-2}\ s^{-1}$) is one of the important

https://doi.org/10.5194/bg-2023-140
Preprint. Discussion started: 22 September 2023

and sensitive parameters to influence the photosynthesis rate of plants and estimate the carbon fluxes (Croft et al., 2017; Luo et al., 2019). V_{cmax} mainly depends on V_{cmax25} and air temperature (T_a, °C) in BEPS model, see supplementary section Text S1 (Eq. S4). Generally, V_{cmax25} is a commonly defined constant among different plant functional types (PFTs) in the model. However, V_{cmax25} actually has large spatial variations (Table S2) due to the changes of species composition, soil properties, and climates within the same PFT, even observations showed a 2-3 fold variation in V_{cmax25} for the same PFT (Chen et al., 2022b). As a result, using a PFT with fixed V_{cmax25} in the model may distort the spatial distribution of the GPP simulation (Chen et al., 2022b). Therefore, in this study, we introduced a spatial variation of V_{cmax25} derived from remote sensing data to replace the constant V_{cmax25} in the original BEPS model. The other parameters used in the BEPS model for each plant functional type can be found in Liu et al. (2018), which were specially parameterized for the simulation of the carbon fluxes of terrestrial ecosystems in China based on the flux tower observations (Liu et al., 2013a; Liu et al., 2016; Liu et al., 2013b) and the published literature (Feng et al., 2007; Liu et al., 2015; Zhang et al., 2012).

2.3 Data and processing

(1) Flux tower data

To evaluate the models' performance, we acquired the daily eddy covariance (EC)-derived GPP and NEP from three flux tower sites over the study area (Fig. 1), which was available from the ChinaFLUX network (Yu et al., 2006). The ChinaFLUX has undergone strict data quality control, including coordinate rotation, WPL correction, nighttime flux correction, gap filling, and flux partitioning. For instance, the nighttime CO_2 flux data under low atmospheric turbulence conditions were screened using site-specific thresholds of friction velocity (u*), which was identified following Reichstein et al. (2005), and the NEE was also partitioned into GEP and ER with the method of Reichstein et al. (2005).

(2) Remote sensing data

LAI. The Global Land Surface Satellite (GLASS) LAI product during 2001-2018 was obtained from the University of Maryland. This data was generated using the general regression neural networks (GRNNs) with a spatiotemporal resolution of 0.05° and 8-day (Xiao et al., 2016). The daily LAI at 0.05° resolution was obtained by linear interpolation of the 8-day GLASS LAI, which was used to drive the BEPS model (Wang et al., 2022). The GLASS LAI was used in this study because of its higher accuracy in China's forests compared to other satellite LAI products, such as the GEOVI LAI, etc. (Liu et al., 2018; Xie et al., 2019).

Satellite-derived V_{cmax25} products. We obtained the spatial variation of satellite-derived V_{cmax25} products from the National Ecosystem Science Data Center, National Science & Technology Infrastructure of China, available from 2000 to 2019, with a spatiotemporal resolution of 500m and 8-day. We used an average yearly V_{cmax25} for each pixel that varied from year to year (2001-2018), and it was further resampled to 0.05°×0.05° for driving the model. The V_{cmax25} product was produced by satellite-derived leaf chlorophyll content (LCC) (Xu et al., 2022) and a semi-mechanistic model (Lu et al., 2022). It has been shown to be robust enough to reduce uncertainty in BEPS model simulations (Lu

https://doi.org/10.5194/bg-2023-140
Preprint. Discussion started: 22 September 2023

et al., 2022; Lu et al., 2020; Wang et al., 2020b). More mechanisms for deriving V_{cmax25} from remote sensing data are available in Lu et al. (2022), Luo et al. (2018), and Xu et al. (2022).

Published GPP products. To better estimate the model performance of the BEPS model, we also used five global GPP products generated by different methods to compare with our simulated GPP, which were further aggregated into 0.05°×0.05° for comparison. The five published GPP products include (a) the MODIS GPP (MOD17A2H Version 6) (Running et al., 2015), (b) the EC-LUE GPP generated by a revised light use efficiency model (Zheng et al., 2020), (c) the NIRv GPP produced by near-infrared reflectance (NIR_V) and machine learning method (Wang et al., 2021b), (d) the VPM GPP produced by the Vegetation Photosynthesis Model (VPM) (Zhang et al., 2017), and (e) another published BEPS GPP product, which was also generated by the BEPS model but with independent driving data and globally calibrated parameters (Chen et al., 2019b; He et al., 2021b). See Table S3 for more details on the five GPP products.

(3) Climate data

We obtained the daily meteorological data including the temperature, precipitation, relative humidity, and downward solar radiation from the Climate Meteorological Forcing Dataset (CMFD) (He et al., 2020), and used it to drive the BEPS model. The CMFD is a high spatial (about 0.1°) and temporal (e.g., hourly and daily) resolution reanalysis product and covers the period of 1979-2018, which has been evaluated against the in-situ meteorological data (He et al., 2020) and widely used in previous studies (Huang et al., 2021; Wang et al., 2020a; Yang et al., 2017a). To ensure consistency with other the resolution of the other drivers, the CMFD was also resampled to 0.05° based on the bilinear interpolation method.

(4) Land cover data

The annual land cover data sets from the European Space Agency (ESA) were used for simulations (ESA, 2017). The ESA CCI land cover data has a resolution of 300 meters, spanning the 1992-present period. The overall global accuracy of CCI land cover data is nearly 75.4%, with higher accuracy for forests (ESA, 2017). In this study, the original CCI land cover data were first aggregated into 0.05°×0.05° by using the CCI LC user tool. Considering the CCI land cover data composed of 37 original classes, we referred to (Tagesson et al., 2020) to reclassify the CCI land cover data into 9 classes, including the evergreen broadleaved forest (EBF), evergreen needleaved forest (ENF), deciduous broadleaved forest (DBF), and mixed forest (MF), cropland (CRO), grassland (GRA), shrubland (SHR), urban (URB), and barren land (BAR).

(5) Soil and atmospheric CO_2 data

The available water capacity (AWC) data with a spatial resolution of 0.05° was extracted from the re-gridded Harmonized World Soil Database (RHWSD) v1.2 (FAO, 2012; Wieder et al., 2014) and used to drive the model in this study. We obtained the annual mean atmospheric CO_2 concentration data (2001-2018) from the Hawaiian Mauna Loa observatory.

https://doi.org/10.5194/bg-2023-140
Preprint. Discussion started: 22 September 2023

2.4 Experiment design

To understand the individual and combined effects of forest cover change, vegetation structure change, CO_2 fertilization, and climate change on annual forest GPP variations during 2001-2018, we designed five groups of simulations in this study (Table 1). First, in scenario $S_{baseline}$, the model was run based on all the dynamic inputs during 2001-2018, including the dynamic land cover, LAI, CO_2, and all climate variables. In scenario S_1, we fixed the land cover in 2001 and allowed all other driven data to vary from 2001 to 2018. It should be noted that in this scenario, land cover change may lead to changes in LAI and thus forest GPP, such as the conversion of forest to non-forest or vice versa, however, the direct cause of LAI change in this scenario is actually due to forest cover change, thus in the present study we set this part of GPP change as the contribution of land cover change (Chen et al., 2021a). In scenario S_2, we conducted four different simulations to investigate how the key climatic factors ($S_{2.1}$: precipitation; $S_{2.2}$: temperature; $S_{2.3}$: solar radiation) and all climate change ($S_{2.4}$) influence the forest GPP. We individually fixed the precipitation, temperature, solar radiation, and all climatic factors in the year 2001, while allowed all other factors (i.e., land cover, LAI, and CO_2) to change over time. In scenario S_3, the LAI was fixed at the level of 2001 and other factors were changed over time. In scenario S_4, we fixed CO_2 concentration (371.31 ppm) in 2001, with other drivers being dynamics. Finally, the difference between $S_{baseline}$ and different scenarios was calculated for estimating the effect of different drivers on forest GPP changes.

Table 1 Design of the scenarios for unravelling the effect of forest cover change, vegetation structure change, CO_2 fertilization, and climate change on forest GPP variations.

Scenarios		Land cover	LAI	Climate	Atmospheric CO_2	Purpose
$S_{baseline}$		Dynamic	Dynamic	Dynamic	Dynamic	Estimating actual dynamics of forest GPP
S_1		Fixed in 2001	Dynamic	Dynamic	Dynamic	Estimating the effect of forest cover change on forest GPP
S_2	**$S_{2.1}$**	Dynamic	Dynamic	Fixed in 2001	Dynamic	Estimating the effect of precipitation on forest GPP
	$S_{2.2}$	Dynamic	Dynamic	Fixed in 2001	Dynamic	Estimating the effect of temperature on forest GPP
	$S_{2.3}$	Dynamic	Dynamic	Fixed in 2001	Dynamic	Estimating the effect of radiation on forest GPP
	$S_{2.4}$	Dynamic	Dynamic	Fixed in 2001	Dynamic	Estimating the effect of climate change on forest GPP
S_3		Dynamic	Fixed in 2001	Dynamic	Dynamic	Estimating the effect of vegetation structural change on forest GPP
S_4		Dynamic	Dynamic	Dynamic	Fixed in 2001	Estimating the effect of CO_2 fertilization on forest GPP

2.5 Statistical analysis

Three statistical metrics were used to assess the performance of the BEPS model in the simulation of GPP and NEP. These metrics include the coefficient of determination (R^2), the root mean square error

https://doi.org/10.5194/bg-2023-140
Preprint. Discussion started: 22 September 2023

(RMSE), and the mean bias error (MBE).

The average values of 3 × 3 pixels centered around the flux sites (provided that these grid pixels have the same land cover type) were used to validate the predicted GPP and NEP (Peng et al., 2021; Wang et al., 2022). In addition, the linear regression analysis was used to detect the long-term trend of the differences between the real and control experiments, which was considered as the impact of the controlled variable on the forest GPP changes.

3. Results

3.1 Model performance

We first compared the simulated daily GPP with the flux-site GPP (Fig. 2). The overall accuracy of GPP simulated by the BEPS model agreed well with measurements from the three flux sites (ALS: R^2 = 0.58, RMSE = 1.57 gC m^{-2} day^{-1}, and MBE = 0.03 gC m^{-2} day^{-1}; DHS: R^2 = 0.44, RMSE = 1.17 gC m^{-2} day^{-1}, and MBE = 0.25 gC m^{-2} day^{-1}; QYZ: R^2 = 0.77, RMSE = 1.36 gC m^{-2} day^{-1}, and MBE = 0.05 gC m^{-2} day^{-1}) (Fig. 2a-c). The BEPS model also showed good performance in simulating daily GPP each year (Table S4, Fig. S1-S3). For example, the R^2 ranged between 0.50 and 0.72 for ALS (2009-2013), ranged between 0.43 and 0.65 for DHS (203-2010), and ranged between 0.70 and 0.85 for QYZ (203-2010). We further examined the BEPS model in simulating daily NEP, which also showed the BEPS model agreed reasonably well with measured daily NEP (Table S5, Fig. S4-S6). The overall accuracy (R^2) of simulated daily NEP was 0.25 (ALS), 0.35 (DHS), and 0.42 (QYZ), respectively (Table S5). However, the simulation accuracy of NEP was generally lower than that of GPP (Table S4-S5). Simulated GPP also captured both the absolute values and the inter-annual variability of observed annual GPP for the three flux sites (Fig. 2d-f). Compared with the yearly measured GPP, the overall accuracy (R^2) of GPP simulated by the BEPS model was 0.89 (ALS), 0.53 (DHS), and 0.73 (QYZ), respectively (Fig. 2 d-f).

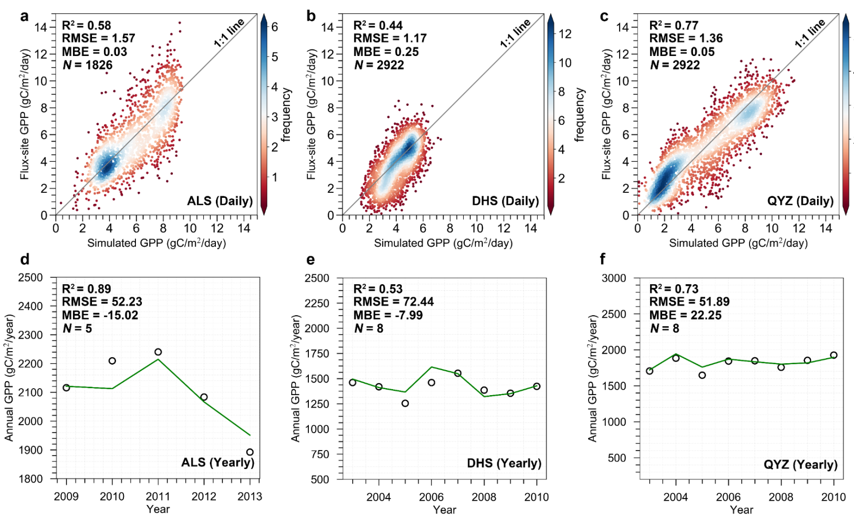

Figure 2 Comparison of simulated GPP with measured GPP from three flux tower stations at daily (a-c) and annual (d-f) scales.

https://doi.org/10.5194/bg-2023-140
Preprint. Discussion started: 22 September 2023

At the regional level, the BEPS model significantly ($p < 0.05$) captured the spatial gradient in GPP compared with the independent products (Fig. 3). The mean R^2 values between our simulated GPP and NIRv GPP, EC-LUE GPP, MODIS GPP, BEPS GPP, and VPM GPP were 0.52, 0.67, 0.41, 0.54, and 0.41, respectively (see Fig. S7f). Especially, the simulated GPP was well consistent with the spatial pattern of the EC-LUE GPP (Fig. S7). In nearly 67% and 34% of forest areas, the R^2 was higher than 0.6 and 0.8, respectively. Besides, we compared the multi-year mean of annual total GPP in our study with the other five GPP products among the entire forest and different forest types (Fig. S8). The multi-year mean of annual total GPP for the entire forest area in our study is 2.23 ± 0.14 PgC year^{-1}, which falled in the range of the five GPP products (i.e., NIRv GPP: 1.66 ± 0.09 PgC year^{-1}; EC-LUE GPP: 1.83 ± 0.09 PgC year^{-1}; VPM GPP: 2.05 ± 0.10 PgC year^{-1}; MODIS GPP: 2.10 ± 0.07 PgC year^{-1}; another BEPS GPP product: 2.54 ± 0.16 PgC year^{-1}) and was also closed to the mean of the five GPP products (2.07± 0.11 PgC year^{-1}) (Fig. S8). Meanwhile, for the entire and different forests, the annual GPP of this study and other GPP products also showed a similar increasing trend (Fig. S8f-8j), such as the trend of the entire forests in this study (0.026 PgC year^{-1}, $p < 0.001$) was closed to the BEPS GPP (0.028 PgC year^{-1}, $p < 0.001$) and the VPM GPP (0.017 PgC year^{-1}, $p < 0.001$) (Fig. S8f). Overall, all the evaluations indicated that the performance of the BEPS model was reasonably well in simulating GPP in the study area.

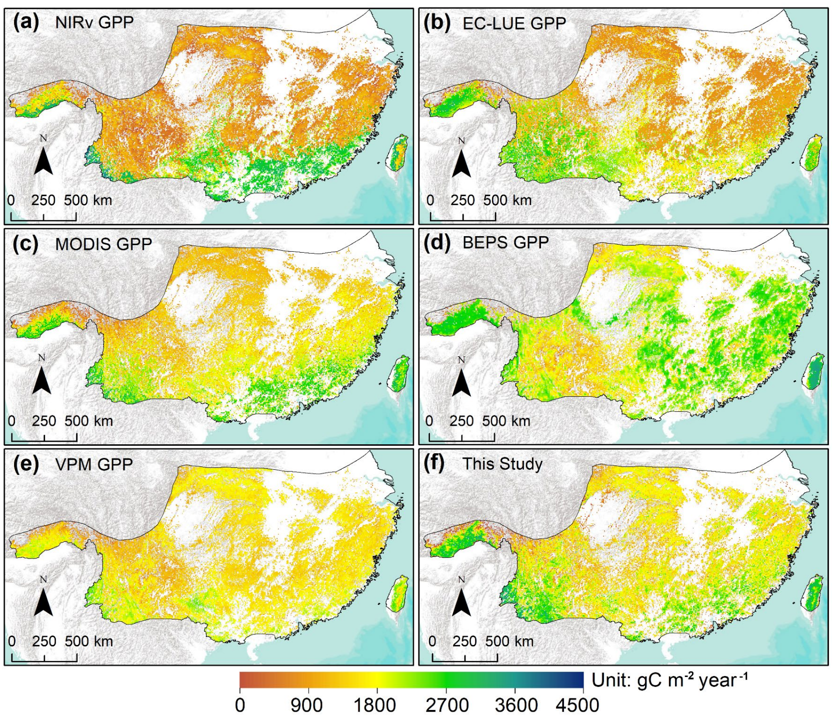

Figure 3 Comparison of the spatial distribution of the mean annual GPP. (a) NIRv GPP, (b) EC-LUE GPP, (c) MODIS GPP, (d) another published BEPS GPP, and (f) our simulated GPP. All the maps were calculated over the 2001–2018 period, except for VPM GPP which is only available from 2001 to 2016.

https://doi.org/10.5194/bg-2023-140
Preprint. Discussion started: 22 September 2023

3.2 Spatiotemporal variations of the actual subtropical forest GPP

The simulated actual GPP showed a significant increasing trend (26.72 TgC year^{-1}, p = 0.000) during 2001-2018 over the entire subtropical forests due to the interactive effect of different drivers (Fig. 4a). Among the four forest types, the EBF showed the largest significantly increasing trend (14.78 TgC year^{-1}, p = 0.000), followed by the MXF (6.46 TgC year^{-1}, p = 0.000), ENF (3.92 TgC year^{-1}, p = 0.000), and DBF (1.55 TgC year^{-1}, p = 0.000). Spatially, 90.4% and 9.6% of the forest GPP showed increased and decreased, respectively (Fig. 4b). Among them, the significantly increased and decreased GPP respectively accounted for 70.1% and 2.6% of the total subtropical forest area (Fig. 4b).

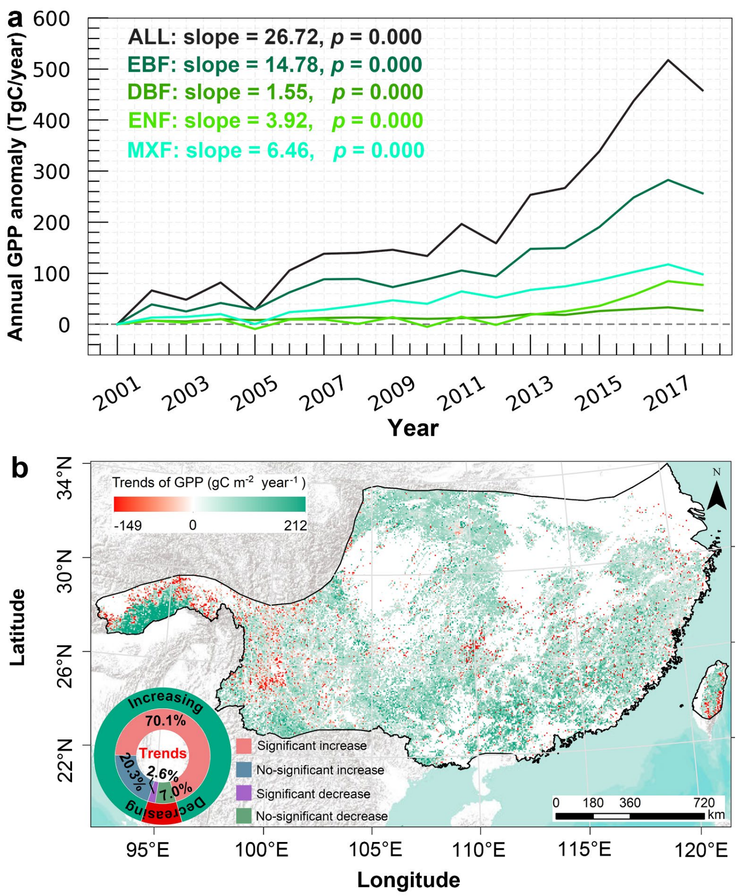

Figure 4 (a) Temporal variations of the annual subtropical forest GPP anomaly during 2001-2018, and the annual GPP anomaly is relative to the base year of 2001; (b) Spatial distribution of the annual trends in actual forest GPP.

3.3 Disentangling the effects of driving factors on forest GPP changes

3.3.1 Impacts of forest cover change on forest GPP changes

Based on the ESA CCI land cover data between 2001 and 2018, it showed that the EBF and MXF had a net increase of 17,340 km^2 and 11,660 km^2, respectively, while the ENF showed a negative net

https://doi.org/10.5194/bg-2023-140
Preprint. Discussion started: 22 September 2023

change (-16,580 km^2) and the DBF was almost unchanged between 2001 and 2018 (Fig. 5). As a whole, the total forest area in our study area showed a net increase change of 12,800 km^2 (Fig. 5a). We found that FCC positively affected the entire forest GPP at a rate of 1.35 TgC year^{-1} (p = 0.000) (Fig. 5b), mainly driven by EBF GPP (1.17 TgC year^{-1}, p = 0.001) and MXF GPP (2.15 TgC year^{-1}, p = 0.000). However, the FCC had a negative effect on the DBF GPP and ENF GPP variations at the rate of -0.05 TgC year^{-1} (p = 0.195) and -1.92 TgC year^{-1} (p = 0.000), respectively. Spatially, 92.2% of the total forest GPP showed a stable state, and only 7.8% of GPP exhibited an increase or decrease under the effect of FCC (Fig. 5c). Among them, 3.9% of the forest GPP increased significantly, mainly located in the western region (e.g., the south slope of the Qinling mountains, the southwest karst region), while 2.6% of the forest GPP was significantly reduced in the eastern regions, which belong to the ENF (Fig. 5).

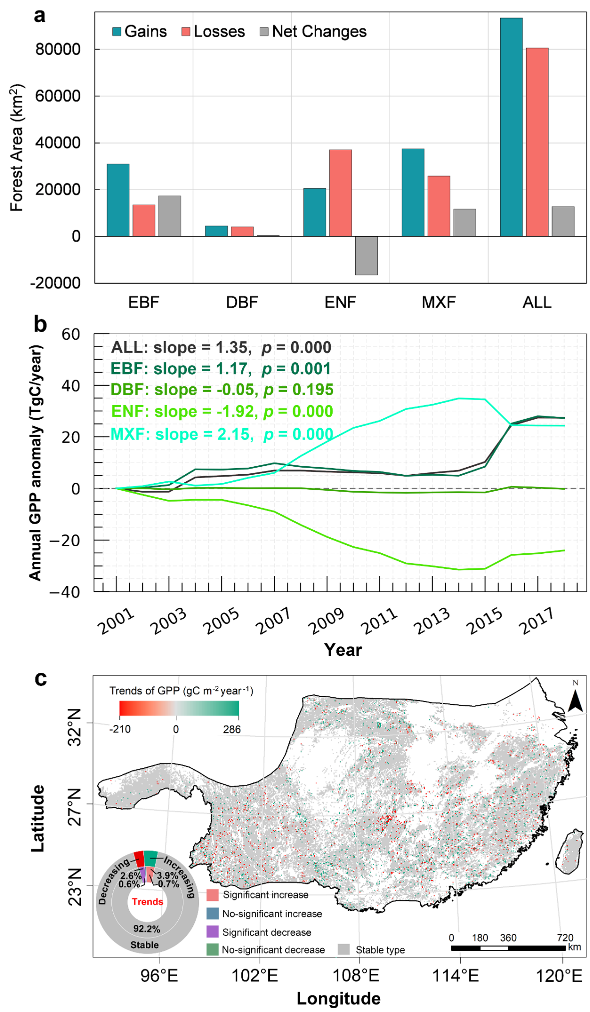

Figure 5 (a) Changes in forest areas between 2001 and 2018. (b) Temporal variation of the effect of forest cover change on annual forest GPP changes. (c) Spatial distribution of the impacts of forest cover change on forest GPP.

https://doi.org/10.5194/bg-2023-140
Preprint. Discussion started: 22 September 2023

3.3.2 Impacts of climate change on forest GPP changes

The annual total precipitation and annual mean temperature over the entire forest region and different forest areas showed an increasing trend (Fig. S9a-S9d), especially the annual mean temperature in the MXF region exhibited a significant upward trend during 2001–2018. By contrast, the annual total radiation displayed a decreasing trend for the entire forest region and different forest areas (Fig. S9e and S9f).

Simulation results showed that an increase in precipitation induced the GPP enhancement at the rate of 0.26 TgC year^{-1} (p = 0.541) for all the forest types together (Fig. 6a). The negative effect of precipitation on ENF GPP (-0.02 TgC year^{-1}, p = 0.618) and MXF GPP (-0.14 TgC year^{-1}, p = 0.137) was mainly offset by EBF GPP (0.33 TgC year^{-1}, p = 0.304) and DBF GPP (0.09 TgC year^{-1}, p = 0.013) enhancements (Fig. 6a). Spatially, the positive effect of precipitation on GPP changes accounted for most parts of the total area (87.5%), of which 3.1% showed a significant (p < 0.05) increase, mainly located in the west and north, which was consistent with the trends in the spatial distribution of precipitation (Fig. S9b). Precipitation also caused a small part of GPP (12.5%) decrease, and there is almost no significant decrease trend (Fig. 6b). Changes in temperature slightly increased the GPP across all forest types (Fig. 6c), but it showed great spatial variations (Fig. 6d). The significantly negative effect of temperature on GPP (13.3%) was mainly distributed in the south and west, while the significantly positive effect of temperature on GPP (8.9%) was mainly located in the western mountainous areas (Fig. 6d). Decreasing solar radiation (Fig. 6e) led to the negative impact of all the forest area (-1.13 TgC year^{-1}, p = 0.162) as well as different forest types (EBF: −0.35 TgC year^{-1}, p = 0.263; DBF: −0.05 TgC year^{-1}, p = 0.442; ENF: −0.51 TgC year^{-1}, p = 0.126; MXF: −0.22 TgC year^{-1}, p = 0.201). The decrease in solar radiation caused a significant decrease in GPP of 10.1% (p < 0.05) (Figure 6f). A small portion of the study areas exhibited GPP enhancement under the influence of solar radiation, but it was hardly significant (3.3%).

Ultimately, the combined and interactive effects of climate change resulted in an increase in GPP across the entire forest area (1.11 TgC year^{-1}, p = 0.080), especially a significant increase in the EBF (1.76 TgC year^{-1}, p = 0.000) and DBF (0.18 TgC year^{-1}, p = 0.003), while the climate change led to the decrease in ENF (-0.53 TgC year^{-1}, p = 0.016) and MXF (-0.29 TgC year^{-1}, p = 0.792) (Fig. 6g). Nearly 41.8% of the study area exhibited an upward trend due to the effect of climate change, mainly distributed in the west and the north (Fig. 6f), of which 10.3% showed a significant (p < 0.05) increase. On the contrary, 58.2% of the study area (a significant area accounted for 6.4%) showed a decreasing trend, mainly located in the east, central, and southwest (Fig. 6f). Overall, the increase in forest GPP induced by precipitation, temperature, and solar radiation can erase their negative effects on GPP, making climate change contribute to forest GPP increase in the whole study area. Although all the main climatic factors did not change significantly during the study period, their combined and interactive effects would have a significant impact on different forest GPP changes (Fig. 6g and 6h), suggesting that different forest GPP has a different sensitivity to climate change.

https://doi.org/10.5194/bg-2023-140
Preprint. Discussion started: 22 September 2023

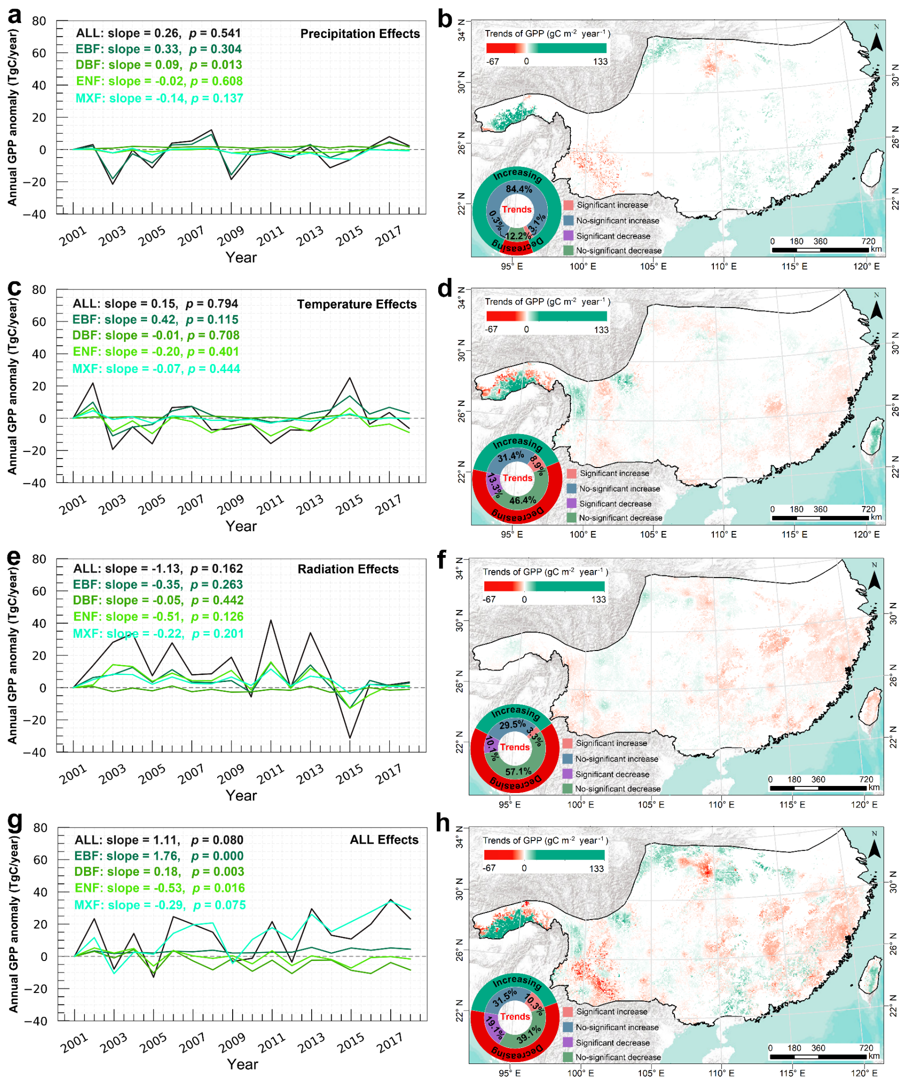

Figure 6 Temporal variation of the effects of precipitation (a), temperature (c), solar radiation (e), and all climate changes (g) on annual GPP trends. Spatial distribution of the impacts of precipitation (b), temperature (d), solar radiation (f), and all climate changes (h) on forest GPP.

3.3.3 Impacts of vegetation structural change on forest GPP changes

The LAI of entire and different forests showed significant upward trends during the study period (Fig. S10). The simulations showed that the VSC exerted a significant positive effect of 4.55 TgC year^{-1} (p = 0.005) for the entire forest region (Fig. 7a), confirming the positive role of VSC in forest GPP variations. Especially, the positive effect of VSC on EBF (1.64 TgC year^{-1}, p = 0.025) contributed the most to the GPP increment (Fig. 7a). There was significant spatial heterogeneity in the effect of VSC on GPP changes (Fig. 7b). A positive effect of VSC on GPP was observed over 68.7% of all forest types

https://doi.org/10.5194/bg-2023-140
Preprint. Discussion started: 22 September 2023

together, where GPP increased significantly ($p < 0.05$) in 29.9% of the total study area. Most of the significantly increasing areas were located in the south and north (Fig. 7b). The areas with a significant decreasing trend ($p < 0.05$) accounted for 6.0%, and they were mainly distributed in the western and central parts of the study area (Fig. 7b). Overall, the results showed that most GPP increases in China's subtropical forests due to the increase of LAI, which also offset the negative effects of VSC on GPP, thus allowing VSC to play a key driving factor in promoting GPP increases throughout the forest area.

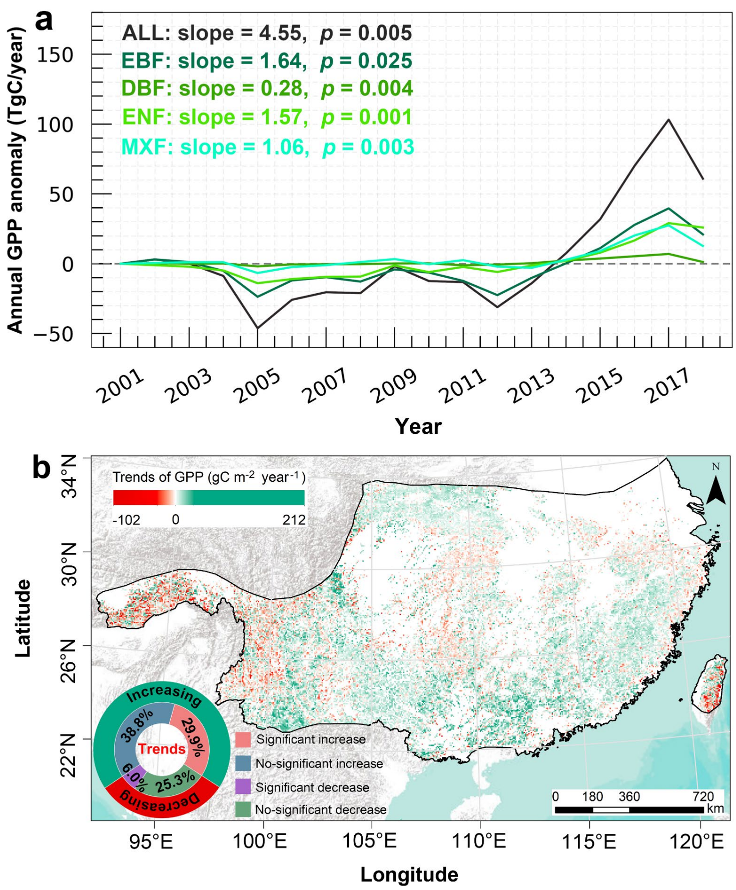

Figure 7 Temporal variation (a) and spatial distribution (b) of the effects of VSC on forest GPP.

3.3.4 Impacts of CO_2 fertilization on forest GPP changes

The annual mean CO_2 concentration increased from 371.3 ppm to 408.7 ppm from 2001 to 2018 (Fig. S11), which led to a significant increase of all forest GPP at the rate of 8.23 TgC year^{-1} ($p = 0.000$) (Fig. 8a). The significantly positive effects of CO_2 fertilization on EBF GPP (3.17 TgC year^{-1}, $p = 0.000$) and ENF GPP (3.06 TgC year^{-1}, $p = 0.000$) was higher than that of DBF GPP (0.42 TgC year^{-1}, $p = 0.000$) and MXF GPP (1.58 TgC year^{-1}, $p = 0.000$). Almost all the China's subtropical forests showed significant positive effects of CO_2 fertilization on GPP (nearly accounting for 99.48% of the total forest area) (Fig. 8b), suggesting the high sensitivity of forests in this area to elevated CO_2.

https://doi.org/10.5194/bg-2023-140
Preprint. Discussion started: 22 September 2023

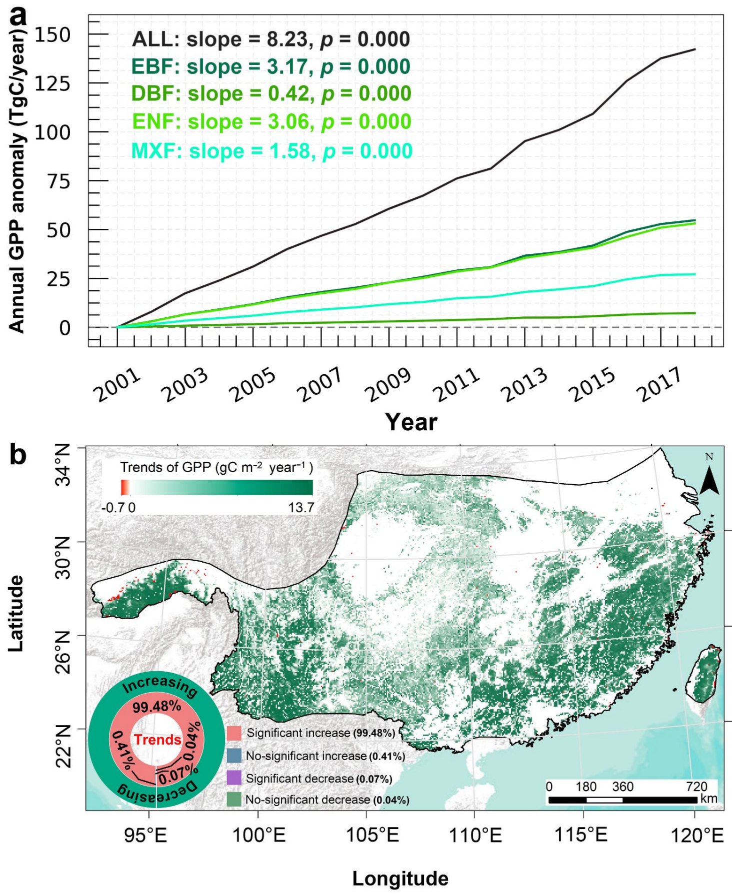

Figure 8 (a) Temporal variation and (b) spatial distribution of the effects of CO_2 fertilization on forest GPP.

3.3.5 Comparison of effects among FCC, CC, VSC, and CO_2 fertilization and the dominant drivers

We compared how different drivers contribute to annual trends in different actual forest GPP (Fig. 9). For all forests together, the enhanced CO_2 concentration made the largest contribution to the overall forest GPP enhancement, followed by VSC, FCC, and CC (Fig. 9a). In addition to the CO_2 fertilization effect, vegetation structure change was another most dominant contributor to actual forest GPP increase across the entire and different forest types (Fig. 9b-9e), especially the positive effect of vegetation structure change almost counteracts the negative effect of forest cover change on ENF GPP. The forest cover change, as the dominant factor, mainly contributed to MXF GPP increase (Fig. 9e), but contributed to the ENF GPP decrease (Fig. 9d). Climate change increased the broad-leaved forests (EBF and DBF) GPP (Fig. 9b and 9c), but it decreased the ENF GPP and MXF GPP (Fig. 9d and 9e). Overall, the EBF in the subtropical region of China has the highest carbon uptake potential in the regulation of the regional carbon cycle (Fig. 9b).

https://doi.org/10.5194/bg-2023-140
Preprint. Discussion started: 22 September 2023

Biogeosciences
Discussions
Open Access

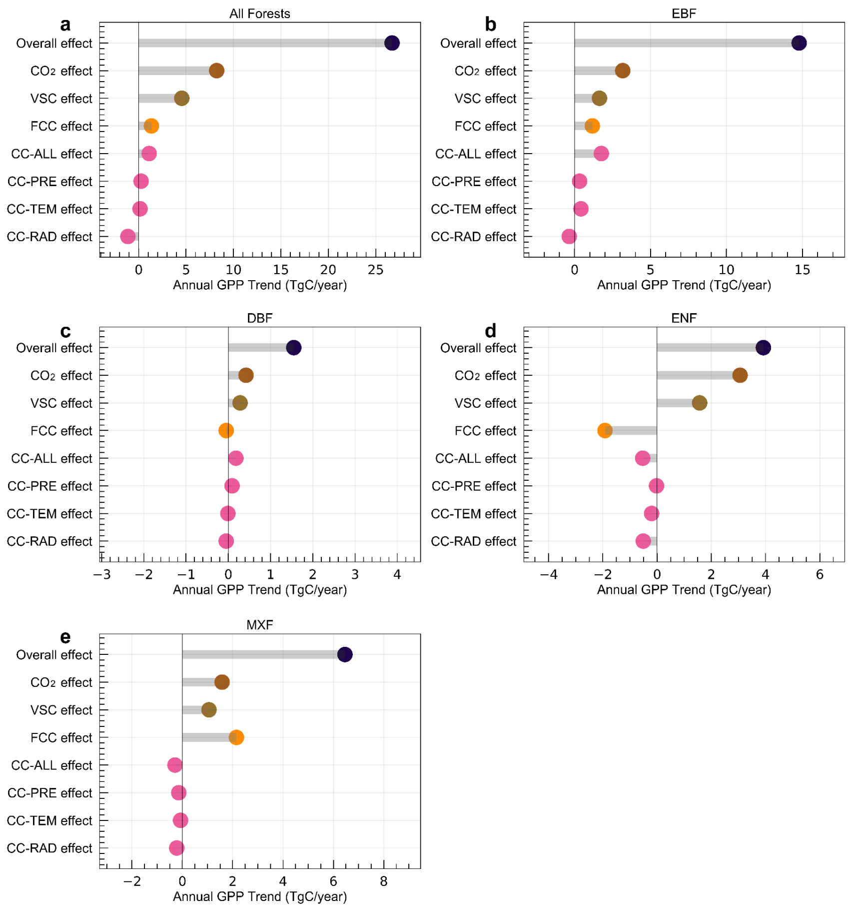

Figure 9 Comparison of different drivers to trends in GPP for entire (a) and different forests (b-e). The overall effect denotes the combined effect of all driving factors; the VSC effect indicates the impact of vegetation structural change on forest GPP. FCC effect indicates the effect of forest cover change on GPP; CC-ALL, CC-PRE, CC-TEM, and CC-RAD respectively represent the impacts of all climatic factors, precipitation, temperature, and solar radiation on forest GPP variations.

We also investigated the spatial distribution of the dominant factors for subtropical forest GPP trends over each grid cell as illustrated in Fig. 10. It was observed that a great variation in the spatial distribution of the dominant factors on forest GPP (Fig. 10). The CO_2 fertilization (41.7%) and VSC (35.7%) were the two dominant factors of forest GPP changes in most regions (Fig. 10). However, the CC (8.9%) was the dominant factor driving forest GPP to increase in the western and northern mountainous areas, and the FCC (4.6%) was the dominant driver of forest GPP decrease in the east.

https://doi.org/10.5194/bg-2023-140
Preprint. Discussion started: 22 September 2023

Biogeosciences Discussions

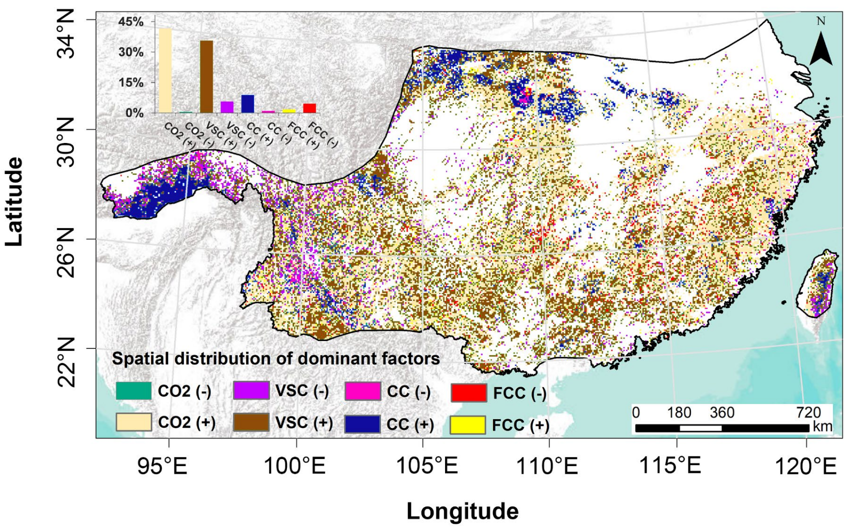

Figure 10 Spatial distribution of the dominant factors on forest GPP changes. (+) and (–) denote the positive and negative effects of these factors on GPP trends, respectively.

4. Discussion

4.1 The effects of the FCC, CC, VSC, and CO_2 fertilization on subtropical forest GPP variation

Overall, the actual GPP of the entire forest region, as well as different forest types, displayed an increasing trend over the past two decades (Fig. 4), which is in line with many previous findings (Chen et al., 2021b; He et al., 2019; Li et al., 2022; Tong et al., 2018). The results also confirmed that the subtropical forests in China have a high carbon sequestration potential under the background of global change. However, there were obvious differences between these factors that contribute to the forest GPP enhancement.

4.1.1 The effect of FCC on forest GPP

In the past two decades, the Chinese government has made an enormous investment to implement some key ecological restoration programs to improve the forest areas, such as the Grain for Green Program (GGP, initiated in 2000) and the Yangtze and Pearl River Basin Shelterbelt programs (Viña et al., 2016; Zhang et al., 2022). The nationwide field samplings confirmed the increment of vegetation cover and carbon sink via these ecological projects since the end of the 20th century (Lu et al., 2018). Especially, the forest restoration hotspots were observed in the south slope of the Qinling Mountains (Chen et al., 2021b) and the southwest karst region (Tong et al., 2018) of China. In similar regions, we also observed that the positive effect of FCC on GPP increased (Fig. 5c). This is due to the increase in the total area of EBF and MXF (Fig. 5a), which is mainly converted from cropland, as shown in the land cover change matrix (Table S6).

The previous studies (Chen et al., 2021a; Chen et al., 2021b; Zhang et al., 2022) usually considered different forests in China as a single forest type, which may ignore the negative effect of a specific forest type on forest GPP variations. In this study, we identified the positive effect (1.35 TgC year^{-1}) of FCC on GPP for all subtropical forest types together. However, disagreements with previous results were also witnessed. The total area of the ENF was lost obviously during the study period in eastern and southern regions, and most of the ENF was also converted to non-forest lands such as cropland and urban (Table S6), causing large parts of GPP to decrease (Fig. 5c). Therefore, this side effect may go unnoticed if different forest types are not considered. For example, the negative effect (-1.92 TgC year^{-1}) of the reduction in ENF area in the eastern and southern regions was more than offset by the positive effect (total: 3.32 TgC year^{-1}) of EBF and MXF cover change on GPP in most regions (Fig. 5b-5c). Therefore, under the influence of FCC, the entire subtropical forest GPP showed an increasing trend (1.35 TgC year^{-1}) (Fig. 5b). Additionally, previous studies generally lumped the land cover change and land use change (LUCC) together and concluded that LUCC is a dominant driver for promoting the forest GPP increase in southern China. However, it may largely ignore the huge contribution of land use change (e.g., forest growth and regeneration) to GPP increase, even when forest cover is unchanged, thereby overstating the role of increased forest area in carbon sequestration in China (Chen et al., 2021a). For instance, Zhang et al. (2022) reported that the reduction of forest cover area instead induced GPP to increase during 2001-2010 in a similar study area, which actually benefited from the contribution of the forest growth (i.e., the increase of the LAI) due to reasonable forest management, instead of forest cover change. Therefore, distinguishing the relative contributions of land cover change and land use change to forest GPP is an essential task.

4.1.2 The effect of CC on forest GPP

Under the combined effect of all climatic factors, an overall increase (1.11 TgC year^{-1}) in forest GPP was observed in the study area (Fig. 6g). However, different climatic factors play different roles in regulating forest GPP changes (Fig. 6a-6f). The precipitation increased forest GPP of the entire study area (0.26 TgC year^{-1}) (Fig. 6a), especially in the northern and western mountains. This is because the slight increase in precipitation in these areas, without exceeding a certain threshold, can increase the soil water content and alleviate the impact of drought stress on forest growth, thereby facilitating forest photosynthesis and enhancing the GPP (He et al., 2019; Li et al., 2022). Temperature is another complex driver of forest GPP variation. Many studies suggested that an increment in temperature can benefit the vegetation productivity, or could reduce the vegetation productivity such as the effect of drought. Our findings also proved that the effect of temperature on forest GPP varied spatially. Most of the region (59.7%) experienced a decline in forest GPP due to the effects of climate warming, while 40.3% of the forest GPP located in the western mountains displayed a significant upward trend (Fig. 6d). This is because the increase in temperature in mountainous areas with high altitudes can extend the growing season and enhance photosynthesis (Nemani et al., 2003; Piao et al., 2005; Zhang et al., 2014), thereby improving the forest GPP. On the contrary, the solar radiation in this study showed a downward trend (Fig. S9e). As a direct limiting factor of vegetation growth, the reduction of solar radiation can directly affect forest photosynthesis, thus declining the forest GPP. As expected, solar radiation in this study declined over 67.2% of forest GPP of the total area (Fig. 6e-6f), which may be associated with the recent increase in air pollution in China (Chen et al., 2021a; Zhang et al., 2014). The combined effects of these climatic factors caused a positive effect (1.11 TgC year^{-1}) on the entire forest GPP (Fig. 6). However,

https://doi.org/10.5194/bg-2023-140
Preprint. Discussion started: 22 September 2023

different forest types showed different responses to climate change (Fig. 6g). For example, climate change has a positive effect on evergreen broadleaved forest GPP, but the negative on evergreen needleleaved forest GPP. Therefore, combating and mitigating climate change should consider different forest types.

4.1.3 The effect of VSC on forest GPP

As the most important proxy of vegetation structure change (VSC) (Chen et al., 2019b; Chen et al., 2021a), LAI can reflect vegetation growth and significantly influence the carbon cycle. Since the 2000s, some key forest protection programs, including the Natural Forest Protection Project (NFPP, initiated in 1998), were carried out in the subtropical region of China (Chen et al., 2020). Due to forest protection and reasonable forest use and management with the support of ecological engineering, forest natural growth has improved the LAI (Chen et al., 2020) and further contributed to the GPP increase in China (Tong et al., 2018). A recent study showed that land-use management in China, especially forest management, has contributed significantly to earth greening, accounting for 25% of the increase in global LAI (Chen et al., 2019a). Chen et al. (2019b) estimated the effect of VSC using the index of LAI on global terrestrial carbon sink since the 1980s, and confirmed that VSC significantly improved the carbon uptake over the global terrestrial ecosystems, especially the VSC promoted the forest carbon sink in China's subtropical region, but the contribution of different forest VSC to GPP changes was not revealed. Evidence from our study demonstrated the VSC as the dominant contributor (4.55 TgC year^{-1}) to the GPP increment of the entire subtropical forests (Fig. 7), and also identified the EBF and MXF were the main contributors to the positive effect of VSC on GPP changes. Recently, although some studies have also demonstrated positive effects of VSC on forest carbon sequestration in China (Chen et al., 2019b; Chen et al., 2020; Zhang et al., 2022), these studies did not isolate the independent effects of VSC on different forest GPP. Therefore, it has been long debated how different ecological projects impact ecosystem services in carbon sequestration (Chen et al., 2020; Yin and Yin, 2010; Yu et al., 2011). Because some ecological projects in China are aimed at protecting forests, others are aimed at increasing forest area. In this study, we designed an experiment to understand the individual impact of VSC (i.e., only reflecting forest structure change) on forest GPP changes. The results showed that forest structure change more than forest cover change positively impacted GPP increases in the study area (Fig. 9a), implying that forest protection projects in the subtropical region of China may have greater carbon uptake potential.

4.1.4 The effect of CO_2 fertilization on forest GPP

Elevated CO_2 concentration can stimulate vegetation photosynthetic rates, thereby enhancing vegetation productivity. Recent studies suggested that the CO_2 fertilization effect was the main driver in promoting global or regional vegetation productivity (Chen et al., 2022a; Chen et al., 2019b; Schimel et al., 2015; Xie et al., 2020). Our results also suggested that CO_2 fertilization was the largest contribution to the overall forest GPP increase in China's subtropical region (8.23 TgC year-1) (Fig. 8). This was also confirmed by observations of the globally distributed eddy covariance networks (Chen et al., 2022a; Zhan et al., 2022). The forests in China are characterized by relatively young stand age (< 40 years old) due to a large number of new plantations, and thus China's forest carbon sequestration potential may continue to increase in the near future due to the rising CO_2 concentration (Yao et al., 2018a). However, there is a lack of dependable and spatially explicit CO_2 concentration data, especially in China, we only used the annual mean CO_2 concentrations from the Mauna Loa Observatory to represent the spatially homogeneous CO_2 concentrations in the study area and to drive the model, which may spatially overestimate or underestimate the effect of CO_2 fertilization on forest GPP (Peng et al., 2022), although it may reasonable to use spatially-uniform and annual average CO_2 concentration to the estimation of large-scale GPP (Chen et al., 2022a; Chen et al., 2021a).

4.2 Model and Uncertainties

In this study, we used the process-based BEPS model to simulate forest GPP of the subtropical region. We first used the V_{cmax25} product retrieved from remote sensing data (i.e., leaf chlorophyll content) to replace the constant value of the V_{cmax25} in the model. Wang et al. (2019), Luo et al. (2018), and Croft et al. (2017) indicated that the use of the remotely sensed leaf chlorophyll content to invert V_{cmax25} can improve the accuracy of GPP simulation in evergreen conifer forests and a temperate deciduous forest. Our results suggested that the BEPS model with spatial varying V_{cmax25} values can also reach reasonable simulation of subtropical forest GPP over spatiotemporal scales (Fig. 2-3, Fig. S1-S6). Incorporating the spatial variation of the V_{cmax25} inverted by remotely sensed data into the process-based model does not require its pre-calibration (Chen et al., 2022b), thus it has great potential to be applied to areas with few flux sites, such as China's subtropical forest area. However, the V_{cmax25} retrieved from remote sensing data is still in the early developing stage (Chen et al., 2022b; Luo et al., 2019), and the high accuracy of spatiotemporal variability of V_{cmax25} products at global and regional scales should be further explored.

In the BEPS model, the LAI is the most important input for carbon fluxes simulation. Previous studies reported large differences in trend and magnitude between existing LAI products over the globe (Fang et al., 2019; Jiang et al., 2017; Liu et al., 2018). Therefore, only the GLASS LAI was used in this study to simulate GPP, which may cause some uncertainty. However, Liu et al. (2018) estimated the accuracy of different satellite-derived LAI products for the simulation of carbon and water fluxes in China's forests based on the BEPS model, and proved that GLASS LAI showed higher accuracy in simulating forest GPP than other LAI products (e.g., FSGOM LAI and MODIS LAI). The consistent conclusions also have been reported in other studies (Chen et al., 2021a; Jiang et al., 2017; Xie et al., 2019). Therefore, it was reasonable to use GLASS LAI as input to model forest GPP in this study.

There are large differences between the available land cover data, such as ESA CCI land cover data (ESA, 2017) and MODIS land cover data (Sulla-Menashe et al., 2019), which were mainly caused by the discrepancies in the definition of forest and divergent data sources (Li et al., 2016; Magdon et al., 2014). Eventually, the use of different land cover data may also lead to uncertainty in the estimate of the regional total GPP. The satellite-derived ESA CCI land cover used in this study may suffer from cloud contamination, satellite signal aliasing, and uncertainty from algorithmic flaws that affect the accuracy of forest cover mapping (Dong et al., 2012). Yang et al. (2017b) systematically evaluated the accuracy of different land cover data in China, showing that ESA CCI data has higher accuracy, especially compared to the commonly used MODIS land cover data. Currently, remote sensing is still considered to be the only effective tool for land cover mapping at large scales, and more precise remote sensing is still needed in the future. Besides, assessing the uncertainties and discrepancies in carbon flux simulations from different land cover data will be the next research work.

5. Conclusions

In this study, the BEPS model was used to simulate the forest GPP. We examined the performance of the BEPS model in simulating subtropical forest GPP, which can reach a high accuracy of GPP simulation in the subtropical forest region of China. A significant increasing trend (26.72 TgC year^{-1}, $p < 0.001$) was detected in the subtropical forest GPP over the past two decades, implying that the subtropical forests have a high carbon sink potential under the background of global change, especially the EBF is the biggest contributor (14.78 TgC year^{-1}, $p < 0.001$) to total GPP enhancement of the entire subtropical forests. We designed different groups of simulations to examine the individual and combined impacts of FCC, CC, VSC, and CO_2 fertilization on inter-annual trends in forest GPP. There are obvious differences in drivers of different forest GPP variations.

Although the CO_2 fertilization effect is the largest contributor to the overall forest GPP increase, the VSC was another most important and not negligible contributor to forest GPP growth in China. The FCC mainly contributed to the MXF GPP increase (2.15 TgC year^{-1}, $p < 0.001$), but induced the ENF GPP to decrease (-1.92 TgC year^{-1}, $p < 0.001$). The CC also increased the EBF and DBF GPP, but it decreased the ENF and MXF GPP. Especially, the forest EBF and DBF GPP in this region are very sensitive ($p < 0.05$) to CC. Therefore, we emphasized that the mitigation of climate change and carbon emissions through forests should consider their different types. Furthermore, our results highlighted the VSC, which was greater than the effects of FCC, was the important driver of the subtropical forest GPP enhancement, suggesting that forest use and management have a more significant positive impact on GPP increase than forest cover change in the study area. It may attribute to the implementation of China's forest protection and restoration programs. Overall, with the support of the government's ecological programs, rational solutions for managing and improving forest structure and function, rather than continuously increasing forest area, may facilitate and maintain the sustainability of the carbon sequestration potential in the study area.

Acknowledgments

This work is jointly supported by the National Natural Science Foundation of China (Grant No. 42171025), the Fonds Wetenschappelijk Onderzoek (FWO Grant n° G018319N), and the program of the China Scholarships Council (Grant No. 202106380124).

Data Availability statement

We obtained the flux tower data from the ChinaFLUX network (http://www.chinaflux.org/), the GLASS LAI from the University of Maryland (http://www.glass.umd.edu/Contact.html), the V_{cmax25} products from the National Ecosystem Science Data Center, National Science & Technology Infrastructure of China (http://www.nesdc.org.cn), the meteorological datasets from the National Tibetan Plateau Third Pole Environment Data Center (https://data.tpdc.ac.cn/en/), the annual land use/cover datasets and the CCI LC user tool from the European Space Agency (ESA) (http://maps.elie.ucl.ac.be/CCI/viewer/), the soil data from the FAO (https://doi.org/10.3334/ORNLDAAC/1247), and the atmospheric CO_2 data

https://doi.org/10.5194/bg-2023-140
Preprint. Discussion started: 22 September 2023

from the National Oceanic and Atmospheric Administration's Earth System Research Laboratories (https://gml.noaa.gov/obop/mlo/).

Author contributions

Conceptualization, methodology, data analysis, writing— original draft, writing—review and editing: TC; conceptualization, methodology, writing— original draft, writing—review and editing: FM. Model, writing— original draft, writing—review and editing: MP. Conceptualization, funding acquisition, project administration, writing—review and editing: GT. Visualization, writing—review and editing: YY. Conceptualization, data analysis, funding acquisition, project administration, writing— original draft, writing—review and editing: HV. All authors have read and agreed to the published version of the manuscript.

Supplement

The supplement related to this article is available online.

Competing interests

The authors declare that they have no known competing financial interests or personal relationships that could have appeared to influence the work reported in this paper.

Disclaimer

Publisher's note: Copernicus Publications remains neutral with regard to jurisdictional claims in published maps and institutional affiliations

References

Barman, R., Jain, A.K. and Liang, M., 2014. Climate-driven uncertainties in modeling terrestrial gross primary production: a site level to global-scale analysis. Global Change Biology, 20(5): 1394-1411.

Beer, C. et al., 2010. Terrestrial Gross Carbon Dioxide Uptake: Global Distribution and Covariation with Climate. Science, 329(5993): 834-838.

Chen, C. et al., 2019a. China and India lead in greening of the world through land-use management. Nature Sustainability, 2: 122-129.

Chen, C., Riley, W.J., Prentice, I.C. and Keenan, T.F., 2022a. CO2 fertilization of terrestrial photosynthesis inferred from site to global scales. Proceedings of the National Academy of Sciences, 119(10): e2115627119.

Chen, J.M., Ju, W., Ciais, P., Viovy, N. and Lu, X., 2019b. Vegetation structural change since 1981 significantly enhanced the terrestrial carbon sink. Nature Communications, 10(1): 4259.

Chen, J.M., Liu, J., Cihlar, J. and Goulden, M.L., 1999. Daily canopy photosynthesis model through temporal and spatial scaling for remote sensing applications. Ecological Modelling 124(2-3): 99–119.

Chen, J.M. et al., 2012. Effects of foliage clumping on the estimation of global terrestrial gross primary productivity. Global Biogeochemical Cycles, 26(1): GB1019.

Chen, J.M. et al., 2022b. Global datasets of leaf photosynthetic capacity for ecological and earth system

https://doi.org/10.5194/bg-2023-140
Preprint. Discussion started: 22 September 2023

research. Earth System Science Data, 14(9): 4077-4093.

Chen, S. et al., 2021a. Vegetation structural change and CO2 fertilization more than offset gross primary production decline caused by reduced solar radiation in China. Agricultural and Forest Meteorology, 296: 108207.

Chen, Y. et al., 2020. Afforestation promotes the enhancement of forest LAI and NPP in China. Forest Ecology and Management, 462: 117990.

Chen, Y. et al., 2021b. Accelerated increase in vegetation carbon sequestration in China after 2010: A turning point resulting from climate and human interaction. Global Change Biology, 27(22): 5848-5864.

CMA, 2018. China Greenhouse Gas Bulletin: The State of Greenhouse Gases in the Atmosphere Based on Chinese and Global Observations before 2017. http://www.cma.gov.cn/en2014/news/News/201901/P020190122575481732415.pdf).

Croft, H. et al., 2017. Leaf chlorophyll content as a proxy for leaf photosynthetic capacity. Global Change Biology, 23: 3513–3524.

Dong, J. et al., 2012. A comparison of forest cover maps in Mainland Southeast Asia from multiple sources: PALSAR, MERIS, MODIS and FRA. Remote Sensing of Environment, 127: 60-73.

ESA, 2017. Land Cover CCI: Product User Guide Version 2.0. [Online]. Available: https://maps.elie.ucl.ac.be/CCI/viewer/download/ESACCI-LC-Ph2-PUGv2_2.0.pdf [Accessed January 15th 2022].

Fang, H., Baret, F., Plummer, S. and Schaepman‐Strub, G., 2019. An Overview of Global Leaf Area Index (LAI): Methods, Products, Validation, and Applications. Reviews of Geophysics, 57(3): 739-799.

Fang, J. et al., 2014. Forest biomass carbon sinks in East Asia, with special reference to the relative contributions of forest expansion and forest growth. Global Change Biology, 20(6): 2019–2030.

Fang, J., Tang, Y. and Son, Y., 2010. Why are East Asian ecosystems important for carbon cycle research? Sci China Life Sci, 53(7): 753–756.

Fang, J., Yu, G., Liu, L., Hu, S. and Chapin, F.S., 2018. Climate change, human impacts, and carbon sequestration in China. Proceedings of the National Academy of Sciences, 115(16): 4015-4020.

FAO, 2012. Harmonized World Soil Database (version 1.2). Food Agriculture Organization, Rome, Italy and IIASA, Laxenburg, Austria (http://webarchive.iiasa.ac.at/Research/LUC/External-World-soil-database/HTML/).

Feng, X. et al., 2007. Net primary productivity of China's terrestrial ecosystems from a process model driven by remote sensing. Journal of Environmental Management, 85(3): 563-573.

Friedlingstein, P. et al., 2022. Global Carbon Budget 2021. Earth System Science Data, 14(4): 1917-2005.

Fyllas, N.M. et al., 2017. Solar radiation and functional traits explain the decline of forest primary productivity along a tropical elevation gradient. Ecology Letters, 20(6): 730–740.

Gao, T., Wang, H.J. and Zhou, T., 2017. Changes of extreme precipitation and nonlinear influence of climate variables over monsoon region in China. Atmospheric Research, 197: 379-389.

He, H. et al., 2021a. Reference carbon cycle dataset for typical Chinese forests via colocated observations and data assimilation. Scientific Data, 8(1): 42.

He, H. et al., 2019. Altered trends in carbon uptake in China's terrestrial ecosystems under the enhanced summer monsoon and warming hiatus. National Science Review, 6(3): 505-514.

He, J. et al., 2020. The first high-resolution meteorological forcing dataset for land process studies over China. Scientific Data, 7(1): 25.

He, Q. et al., 2021b. Drought Risk of Global Terrestrial Gross Primary Productivity Over the Last 40 Years Detected by a Remote Sensing-Driven Process Model. Journal of Geophysical Research: Biogeosciences, 126(6): e2020JG005944.

Huang, J. et al., 2021. Characterizing the river water quality in China: Recent progress and on-going challenges. Water Research, 201: 117309.

Jiang, C. et al., 2017. Inconsistencies of interannual variability and trends in long-term satellite leaf area index products. Global Change Biology, 23(10): 4133-4146.

Ju, W. et al., 2006. Modelling multi-year coupled carbon and water fluxes in a boreal aspen forest. Agricultural and Forest Meteorology, 140(1-4): 136-151.

Li, C. et al., 2014. A Circa 2010 Thirty Meter Resolution Forest Map for China. Remote Sensing, 6(6): 5325-5343.

Li, W. et al., 2016. Major forest changes and land cover transitions based on plant functional types derived from the ESA CCI Land Cover product. International Journal of Applied Earth Observation and Geoinformation, 47: 30-39.

Li, Y., Zhang, Y. and Lv, J., 2022. Interannual variations in GPP in forest ecosystems in Southwest China and regional differences in the climatic contributions. Ecological Informatics, 69: 101591.

Liu, J., Chen, J.M., Cihlar, J. and Chen, W., 1999. Net primary productivity distribution in the BOREAS region from a process model using satellite and surface data. Journal of Geophysical Research: Atmospheres, 104(D22): 27735-27754.

Liu, J., Chen, J.M., Cihlar, J. and PArk, W.M., 1997. A process-based boreal ecosystem productivity simulator using remote sensing inputs. Remote Sensing of Environment, 62(2): 158-175.

Liu, Y. et al., 2013a. Changes of net primary productivity in China during recent 11 years detected using an ecological model driven by MODIS data. Frontiers of Earth Science, 7(1): 112-127.

Liu, Y. et al., 2016. Recent trends in vegetation greenness in China significantly altered annual evapotranspiration and water yield. Environmental Research Letters, 11(9): 094010.

Liu, Y. et al., 2015. Water use efficiency of China's terrestrial ecosystems and responses to drought. Sci Rep, 5: 13799.

Liu, Y. et al., 2018. Satellite-derived LAI products exhibit large discrepancies and can lead to substantial uncertainty in simulated carbon and water fluxes. Remote Sensing of Environment, 206: 174-188.

Liu, Y. et al., 2013b. Evapotranspiration and water yield over China's landmass from 2000 to 2010. Hydrology and Earth System Sciences, 17(12): 4957-4980.

Liu, Y. et al., 2014. Impacts of droughts on carbon sequestration by China's terrestrial ecosystems from 2000 to 2011. Biogeosciences, 11(10): 2583-2599.

Lu, F. et al., 2018. Effects of national ecological restoration projects on carbon sequestration in China from 2001 to 2010. Proceedings of the National Academy of Sciences, 115(16): 4039-4044.

Lu, X., Croft, H., Chen, J.M., Luo, Y. and Ju, W., 2022. Estimating photosynthetic capacity from optimized Rubisco–chlorophyll relationships among vegetation types and under global change.

https://doi.org/10.5194/bg-2023-140
Preprint. Discussion started: 22 September 2023

Environmental Research Letters, 17(1): 014028.

Lu, X. et al., 2020. Maximum Carboxylation Rate Estimation With Chlorophyll Content as a Proxy of Rubisco Content. Journal of Geophysical Research: Biogeosciences, 125(8): e2020JG005748.

Luo, X. et al., 2018. Incorporating leaf chlorophyll content into a two-leaf terrestrial biosphere model for estimating carbon and water fluxes at a forest site. Agricultural Forest Meteorology, 248: 156-168.

Luo, X., Croft, H., Chen, J.M., He, L. and Keenan, T.F., 2019. Improved estimates of global terrestrial photosynthesis using information on leaf chlorophyll content. Global Change Biology, 25(7): 2499-2514.

Ma, J. et al., 2019. Trends and controls of terrestrial gross primary productivity of China during 2000–2016. Environmental Research Letters, 14(8): 084032.

Ma, J., Yan, X., Dong, W. and Chou, J., 2015. Gross primary production of global forest ecosystems has been overestimated. Scientific Reports, 5(1): 10820.

Magdon, P., Fischer, C., Fuchs, H. and Kleinn, C., 2014. Translating criteria of international forest definitions into remote sensing image analysis. Remote Sensing of Environment, 149: 252-262.

Mathias, J.M. and Trugman, A.T., 2022. Climate change impacts plant carbon balance, increasing mean future carbon use efficiency but decreasing total forest extent at dry range edges. Ecology Letters, 25(2): 498-508.

Matsushita, B. and Tamura, M., 2002. Integrating remotely sensed data with an ecosystem model to estimate net primary productivity in East Asia. Remote Sensing of Environment, 81(1): 58-66.

Mo, X., Liu, S., Chen, X. and Hu, S., 2018. Variability, tendencies, and climate controls of terrestrial evapotranspiration and gross primary productivity in the recent decade over China. Ecohydrology, 11(4): e1951.

Nemani, R.R. et al., 2003. Climate-Driven Increases in Global Terrestrial Net Primary Production from 1982 to 1999. Science, 300: 1560-1563.

Pan, Y. et al., 2011. A large and persistent carbon sink in the world's forests. Science, 333(6045): 988-993.

Peng, J. et al., 2022. Overestimated Terrestrial Carbon Uptake in the Future Owing to the Lack of Spatial Variations CO2 in an Earth System Model. Earth's Future, 10: e2021EF002440.

Peng, J. et al., 2021. Incorporating water availability into autumn phenological model improved China’s terrestrial gross primary productivity (GPP) simulation. Environmental Research Letters, 16(9): 094012.

Piao, S. et al., 2005. Changes in vegetation net primary productivity from 1982 to 1999 in China. Global Biogeochemical Cycles, 19(2): GB2027.

Reichstein, M. et al., 2005. On the separation of net ecosystem exchange into assimilation and ecosystem respiration: review and improved algorithm. Global Change Biology, 11(9): 1424-1439.

Running, S.W. and Coughlan, J.C., 1988. A general model of forest ecosystem processes for regional applications I. Hydrologic balance, canopy gas exchange and primary production processes. Ecological Modelling, 42(2): 125-154.

Running, S.W., Mu, Q. and Zhao, M., 2015. MOD17A2H MODIS/Terra Gross Primary Productivity 8-Day L4 Global 500m SIN Grid. NASA LP DAAC. http://doi.org/10.5067/MODIS/MOD17A2H.006.

Schimel, D., Stephens, B.B. and Fisher, J.B., 2015. Effect of increasing CO2 on the terrestrial carbon cycle. Proceedings of the National Academy of Sciences, 112(2): 436-41.

Sprintsin, M., Chen, J.M., Desai, A. and Gough, C.M., 2012. Evaluation of leaf-to-canopy upscaling methodologies against carbon flux data in North America. Journal of Geophysical Research: Biogeosciences, 117: G01023.

Sulla-Menashe, D., Gray, J.M., Abercrombie, S.P. and Friedl, M.A., 2019. Hierarchical mapping of annual global land cover 2001 to present: The MODIS Collection 6 Land Cover product. Remote Sensing of Environment, 222: 183-194.

Tagesson, T. et al., 2020. Recent divergence in the contributions of tropical and boreal forests to the terrestrial carbon sink. Nature Ecology & Evolution, 4(2): 202-209.

Thornton, P.E. et al., 2002. Modeling and measuring the effects of disturbance history and climate on carbon and water budgets in evergreen needleleaf forests. Agricultural and Forest Meteorology, 113(1-4): 185-222.

Tong, X. et al., 2018. Increased vegetation growth and carbon stock in China karst via ecological engineering. Nature Sustainability, 1(1): 44-50.

Viña, A., McConnell, W.J., Yang, H., Xu, Z. and Liu, J., 2016. Effects of conservation policy on China's forest recovery. Science Advances, 2: e1500965.

Wang, B., Ma, Y., Su, Z., Wang, Y. and Ma, W., 2020a. Quantifying the evaporation amounts of 75 highelevation large dimictic lakes on the Tibetan Plateau. Science Advances, 6: eaay8558.

Wang, M. et al., 2018. Detection of Positive Gross Primary Production Extremes in Terrestrial Ecosystems of China During 1982-2015 and Analysis of Climate Contribution. Journal of Geophysical Research: Biogeosciences, 123(9): 2807-2823.

Wang, M., Wang, S., Zhao, J., Ju, W. and Hao, Z., 2021a. Global positive gross primary productivity extremes and climate contributions during 1982-2016. Sci Total Environ, 774: 145703.

Wang, Q. et al., 2003. Simulation and scaling of temporal variation in gross primary production for coniferous and deciduous temperate forests. Global Change Biology 10: 37–51.

Wang, R., Chen, J.M., Luo, X., Black, A. and Arain, A., 2019. Seasonality of leaf area index and photosynthetic capacity for better estimation of carbon and water fluxes in evergreen conifer forests. Agricultural and Forest Meteorology, 279: 107708.

Wang, S. et al., 2020b. Estimation of Leaf Photosynthetic Capacity From Leaf Chlorophyll Content and Leaf Age in a Subtropical Evergreen Coniferous Plantation. Journal of Geophysical Research: Biogeosciences, 125(2): e2019JG005020.

Wang, S., Zhang, Y., Ju, W., Qiu, B. and Zhang, Z., 2021b. Tracking the seasonal and inter-annual variations of global gross primary production during last four decades using satellite near-infrared reflectance data. Sci Total Environ, 755(Pt 2): 142569.

Wang, X., Chen, J.M., Ju, W. and Zhang, Y., 2022. Seasonal Variations in Leaf Maximum Photosynthetic Capacity and Its Dependence on Climate Factors Across Global FLUXNET Sites. Journal of Geophysical Research: Biogeosciences, 127(5): e2021JG006709.

Wieder, W.R., Boehnert, J., Bonan, G.B. and Langseth, M., 2014. Regridded Harmonized World Soil Database v1.2. ORNL DAAC, Oak Ridge, Tennessee, USA. https://doi.org/10.3334/ORNLDAAC/1247.

Xiao, Z. et al., 2016. Long-Time-Series Global Land Surface Satellite Leaf Area Index Product Derived From MODIS and AVHRR Surface Reflectance. IEEE Transactions on Geoscience and Remote

Sensing, 54(9): 5301-5318.

Xie et al., 2018. Derivation of temporally continuous leaf maximum carboxylation rate (V-cmax) from the sunlit leaf gross photosynthesis productivity through combining BEPS model with light response curve at tower flux sites. Agricultural and Forest Meteorology, 259(15): 82-94.

Xie, S., Mo, X., Hu, S. and Liu, S., 2020. Contributions of climate change, elevated atmospheric CO2 and human activities to ET and GPP trends in the Three-North Region of China. Agricultural and Forest Meteorology, 295: 108183.

Xie, X. et al., 2019. Assessment of five satellite-derived LAI datasets for GPP estimations through ecosystem models. Science of the Total Environment, 690: 1120-1130.

Xu, M. et al., 2022. A 21-Year Time Series of Global Leaf Chlorophyll Content Maps From MODIS Imagery. IEEE Transactions on Geoscience and Remote Sensing, 60: 1-13.

Yang, F. et al., 2017a. Evaluation of multiple forcing data sets for precipitation and shortwave radiation over major land areas of China. Hydrology and Earth System Sciences, 21(11): 5805-5821.

Yang, Y., Xiao, P., Feng, X. and Li, H., 2017b. Accuracy assessment of seven global land cover datasets over China. ISPRS Journal of Photogrammetry and Remote Sensing, 125: 156-173.

Yao, Y., Piao, S. and Wang, T., 2018a. Future biomass carbon sequestration capacity of Chinese forests. Science Bulletin, 63(17): 1108-1117.

Yao, Y. et al., 2018b. Spatiotemporal pattern of gross primary productivity and its covariation with climate in China over the last thirty years. Global Change Biology, 24(1): 184-196.

Yin, R. and Yin, G.J.E.M., 2010. China's Primary Programs of Terrestrial Ecosystem Restoration: Initiation, Implementation, and Challenges. Environmental Management 45(3): 429-441.

Yu, D.Y. et al., 2011. Forest ecosystem restoration due to a national conservation plan in China. Ecological Engineering, 37(9): 1387-1397.

Yu, G.-R. et al., 2006. Overview of ChinaFLUX and evaluation of its eddy covariance measurement. Agricultural and Forest Meteorology, 137(3-4): 125-137.

Yu, G. et al., 2014. High carbon dioxide uptake by subtropical forest ecosystems in the East Asian monsoon region. Proceedings of the National Academy of Sciences, 111(13): 4910-4915.

Yuan, W. et al., 2016. Severe summer heatwave and drought strongly reduced carbon uptake in Southern China. Scientific Reports, 6(1): 18813.

Zhan, C. et al., 2022. Emergence of the physiological effects of elevated CO(2) on land-atmosphere exchange of carbon and water. Global Change Biology, 28(24): 7313-7326.

Zhang, F. et al., 2012. Variations of Terrestrial Net Primary Productivity in East Asia. Terrestrial, Atmospheric and Oceanic Sciences, 23(4): 425-437.

Zhang, X. et al., 2022. Land cover change instead of solar radiation change dominates the forest GPP increase during the recent phase of the Shelterbelt Program for Pearl River. Ecological Indicators, 136: 108664.

Zhang, Y. et al., 2014. Effects of land use/land cover and climate changes on terrestrial net primary productivity in the Yangtze River Basin, China, from 2001 to 2010. Journal of Geophysical Research: Biogeosciences, 119(6): 1092-1109.

Zhang, Y. et al., 2017. A global moderate resolution dataset of gross primary production of vegetation for 2000-2016. Scientific Data, 4: 170165.

https://doi.org/10.5194/bg-2023-140
Preprint. Discussion started: 22 September 2023

Zheng, Y. et al., 2020. Improved estimate of global gross primary production for reproducing its long-term variation, 1982–2017. Earth System Science Data, 12(4): 2725-2746.